Journal of Molecular Liquids 349 (2022) 118481

Contents lists available at ScienceDirect

Journal of Molecular Liquids

journal homepage: www.elsevier.com/locate/molliq

Amino acid-based ionic liquids as dual kinetic-thermodynamic methane hydrate inhibitor

Asiah Nusaibah Masri [a,d,e,*], Aliyu Adebayo Sulaimon [a,b,c]

[a] Centre of Research in Ionic Liquids (CORIL), Universiti Teknologi PETRONAS, 32610 Bandar Seri Iskandar, Perak, Malaysia
[b] Centre for Flow Assurance (CFA), Universiti Teknologi PETRONAS, 32610 Bandar Seri Iskandar, Perak, Malaysia
[c] Petroleum Engineering Department, Universiti Teknologi PETRONAS, 32610 Bandar Seri Iskandar, Perak, Malaysia
[d] Energy Engineering Department, School of Chemical and Energy Engineering, Faculty of Engineering, Universiti Teknologi Malaysia, 81310 Skudai, Johor, Malaysia
[e] UTM-MPRC Institute for Oil and Gas (IFOG), School of Chemical and Energy Engineering, Faculty of Engineering, Universiti Teknologi Malaysia, 81310 Skudai, Johor, Malaysia

ARTICLE INFO

Article history:
Received 22 September 2021
Revised 26 December 2021
Accepted 4 January 2022
Available online 7 January 2022

Keywords:
Methane hydrates
Thermodynamic inhibitor
Kinetic inhibitor
Ionic liquid
COSMO-RS
Hydrogen bonding energy

ABSTRACT

Three amino acid-based ionic liquids (AAILs) are synthesized to evaluate their performance as inhibitors. They are 1-ethyl-3-methyl-imidazolium-glutamate (EMIMGlu), 1-(3-cyanopropyl)-3-methyl-imidazolium-glutamate (CPMIMGlu) and 1-butyl-3-methyl-imidazolium-glutamate (BMIMGlu). The structures are clarified using Nuclear Magnetic Resonance. Evaluation of their methane hydrate inhibitor performance is performed by micro-differential scanning calorimeter at 5–15 MPa. As a baseline, the hydrate dissociation in water is also evaluated. A standard correlation of methane hydrate dissociation in water is successfully developed with a low average absolute error. Additionally, the AAILs behave as both thermodynamic (THI) and kinetic (KHI) hydrate inhibitors. They simultaneously shift the HLVE curve to a lower temperature and decelerate the hydrate formation by reducing the hydrate nucleation rate. EMIMGlu shows the highest THI performance by producing an average temperature shift of 1.14 K, followed by CPMIMGlu (0.91 K) and BMIMGlu (0.87 K). Furthermore, the addition of the nitrile group in CPMIMGlu IL has enhanced the kinetic inhibition process. The kinetic inhibition performance represented by the relative inhibition power (RIP) decreases in the trend of CPMIMGlu (1.31), EMIMGlu (1.30) and BMIMGlu (0.063). The mechanism of the inhibition is further studied by utilizing COSMO-RS software through σ-profile and σ-potential to understand the inhibition process at the molecular level. The experimental results and computational studies reveal that AAILs behave as THI and KHI through the existence of four oxygen atoms in their anions and cyano group in the CPMIM cation. Thermodynamic inhibition properties of AAILs are found to be influenced by the polarity of AAILs while the kinetic inhibition properties of AAILs are found to be influenced by the hydrogen-bonding acceptor value of the AAILs.

1. Introduction

Gas hydrates are the crystalline solid structure of water molecules formed through hydrogen bonding containing encapsulated guest molecules (gas) [1]. Gas hydrate can be in three structure forms, depending on the size of encapsulated gas. Structure I usually contains methane, ethane, or carbon dioxide, Structure II contains propane while Structure H contains a mixture of methane and butane [2]. Gas hydrate is the main safety concern in the oil and gas industry, specifically in flow assurance during gas transportation and storage. Gas hydrate may cause pipeline blockages and lead to an explosion, operational shutdown, huge maintenance cost, and environmental hazards [3]. Hence, the industry wastes approximately $200 M annually to hinder their formation [4]. The methane content in the natural gas wells differs depending

Abbreviations: AAIL, Amino acid-based ionic liquid; BF_4, Tetrafluoroborate; BMIM, 1-butyl-3-methylimidazolium; Br, Bromide; B3LYP, Becke 3-parameter Lee-Yang-Parr; CH_4, Methane; Cl, Chloride; CNMR, Carbon nuclear magnetic resonance; COSMO-RS, Conductor-like Screening Model for Real Solvents; CPMIM, 1-(3-cyano propyl)-3-methylimidazolium; DFT, Density functional theory (DFT); EMIM, 1-ethyl-3-methylimidazolium; Glu, Glutamate; HLVE, Hydrate-aqueous liquid-vapor equilibrium; HNMR, Proton nuclear magnetic resonance; ILs, Ionic Liquids; KHI, Kinetic hydrate inhibitor; LuviCap, 40 wt% poly(vinyl caprolactam) in ethylene glycol; NMR, Nuclear magnetic resonance; PVCap, poly(vinyl caprolactam); THI, Thermodynamic hydrate inhibitor; σ-profile, Sigma profile; σ-potential, Sigma potential.

* Corresponding authors.
E-mail addresses: asiahnusaibah2@gmail.com, nusaibah@utm.my (A.N. Masri).

https://doi.org/10.1016/j.molliq.2022.118481
0167-7322/

on the location. The top Asian countries producing methane include China, Saudi Arabia, Turkmenistan, Indonesia, and Malaysia [5].

Several techniques were practised to hinder hydrate formation in the pipeline such as gas stream dehydration, pipeline insulation, and chemical injection [6]. However, gas stream dehydration and pipeline insulation require a high cost in the industry [7]. Hence, chemical injection in the gas stream has been practised [8]. Chemical inhibitors are divided into thermodynamic hydrate inhibitors (THIs) and kinetic hydrate inhibitors (KHIs) or also called low-dosage hydrate inhibitors [9]. The conventional THIs i.e methanol and ethylene–glycol are usually utilized at high concentrations in the range of 10–50 wt% as they are volatile thus increasing the material and storage cost [10]. Additionally, they are toxic thus their release to the environment should be avoided. On the other hand, the conventional KHIs i.e polyvinylpyrrolidone (PVP) and polyvinyl caprolactam (PVCap) are less effective in extreme conditions of a deeper-water pipeline which usually has a lower temperature and higher pressure [11].

Ionic liquids (ILs) are organic salt comprised of cation and anion. They usually appear as a liquid at ambient conditions [12]. Their application has attracted the substantial attention of researchers thanks to their distinct properties. They are high thermal stability [13], high chemical stability [14], high catalytic ability [15], and a simple recovery process [16]. Additionally, they also possess negligible vapour pressure which can resolve the problem of volatile and flammable conventional solvent [17]. Hence, the use of ILs to replace conventional volatile THIs has sparked the interest of several researchers. They are first explored as THIs for methane hydrate by Xiao and Adidharma in 2009 [3]. Xiao and Adidharma found that 1-ethyl-3-methylimidazolium tetrafluoroborate (EMIM BF_4) and 1-butyl-3-methylimidazolium tetrafluoroborate ($BMIMBF_4$) showed better performance in shifting hydrate-aqueous liquid–vapour equilibrium (HLVE) curve compared to conventional polyethylene oxide chemical inhibitor. Moreover, they also found that the ILs were able to behave as KHIs. Their presence expanded the induction time to 6 times longer than conventional Luvicap (40 wt% poly(N-vinyl caprolactam) in ethylene glycol. Since then, various ILs has been evaluated as alternative gas hydrate inhibitors, especially ILs having halide anions [18,19]. However, halide-based ILs are hazardous to the environment [20].

Thus, this research is proposing the use of biodegradable ILs containing glutamate as the anion which is a type of amino acid IL (AAIL) that can be synthesized using glutamic acid, which is a naturally abundant source. Three AAILs, namely 1-ethyl-3-methy l-imidazolium-glutamate (EMIMGlu), 1-cyanopropyl-3- methyl-imidazolium-glutamate (CPMIMGlu) and 1-butyl-3- methyl-imidazolium-glutamate (BMIMGlu), are synthesized and their ability to inhibit methane hydrate is evaluated using micro-DSC in a pressure range of 5–15 MPa. The average temperature shift of the HLVE curve and average induction time are evaluated to describe their thermodynamic and kinetic inhibition ability, respectively. Conductor-like Screening Model for Real Solvent (COSMO-RS) software is used to describe the molecular properties such as polarity and hydrogen bonding strength of the AAILs which affect their hydrate inhibition ability.

2. Materials and methods

2.1. Reagents & materials

All chemicals are commercially available and used as received without further purification unless otherwise stated. The materials are listed in Table 1. Nuclear Magnetic Resonance (^{1}HNMR) analysis is performed using Bruker Advance 500 MHz spectrometer.

Table 1
List of materials.

No.	Material	Purity (%)	Supplier
1	1-ethyl-3-methylimidazolium chloride (EMIMCl)	98	Sigma-Aldrich
2	1-cyanopropyl-3-methylimidazolium chloride (CPMIMCl)	98.5	Sigma-Aldrich
3	1-butyl-3-methylimidazolium chloride (BMIMCl)	98	Sigma-Aldrich
4	Amberlyst A26 hydroxide form resin	45–65% moisture	Supelco
5	Glutamic acid	99	Sigma-Aldrich
6	Methanol	99.8	Sigma-Aldrich
7	Silver nitrate	99.0	Sigma-Aldrich
8	Acetonitrile	99.8	Sigma-Aldrich

2.2. Ionic liquids synthesis

5.0 g of 1-ethyl-3-methyl-imidazolium-chloride (EMIMCl) in 150 mL methanol is slowly added to Amberlyst A26 hydroxide from resin in a burette for 24 h. This allows ion exchange of Cl^- anion and OH^- anion to take place. This intermediate is collected in a conical flask during the ion exchange process. Then, 5.018 g glutamic acid is added to the intermediate and stirred for 24 h. Then, the resulted mixture is tested with a few drops of silver nitrate. No precipitation formation during the test defined that full reactant conversion happened. The remaining solvents (methanol and water) inside the mixture are removed using a rotary evaporator leaving behind the 1-ethyl-3-methylimidazolium glutamate (EMIMGlu) IL as the product. After that, EMIMGlu IL is washed using acetonitrile and methanol to remove traces of impurities. Finally, the washing solvents are removed using a rotary evaporator. The structure of EMIMGlu IL is confirmed by an HNMR spectrometer. ^{1}H NMR for 1-ethyl-3-methylimidazolium glutamate (EMIMGlu): δ ppm 1.403 (t,3H), 1.673 (m,2H), 2.123 (m,2H), 3.120 (t,1H), 3.860 (s,3H), 4.213 (m,2H), 7.735 (d,1H), 7.822 (d,1H) and 9.425 (s,1H).

The 1-(3-cyanopropyl)-3-methylimidazoliumglutamate (CPMIMGlu) and 1-butyl-3-methylimidazoliumglutamate (BMIMGlu) were prepared similarly by substituting EMIMCl with CPMIMCl and BMIMCl, respectively. ^{1}H NMR for 1-(3-cyanopro pyl)-3-methylimidazolium glutamate (CPMIMGlu): δ ppm 1.742 (m,2H), 2.126 (m,2H), 2.154 (m,2H), 2.607 (m,2H), 3.203 (t,1H), 3.862 (s,3H), 4.284 (t,2H), 7.772 (d,1H), 7.850 (d,1H) and 9.525 (s,1H). ^{1}H NMR for 1-butyl-3-methylimidazolium glutamate (BMIMGlu): δ ppm 0.891 (t,3H), 1.255 (m,2H), 1.758 (m,2H), 1.778 (m,2H), 2.143 (m,2H), 3.120 (t,1H), 3.860 (s,3H), 4.175 (t,2H), 7.737 (d,1H), 7.798 (d,1H) and 9.380 (s,1H).

2.3. Methane hydrate inhibition measurements

SETARAM High-pressure Micro Differential Scanning Calorimeter (HP μ-DSC) is used to evaluate the heat flow spectrum over time and temperature with the presence of methane gas. 10 wt% of AAILs in water are tested in a temperature range of 253.15–293.15 K at five pressure points: 5.0, 7.5, 10.0, 12.5, and 15.0 MPa. The sample is cooled down at an initial temperature of 293.15–253.15 K at 0.5 K/min. It is then maintained at 253.15 K for 10 min. Then, the sample is heated up from 253.15 K to 293.15 K at 0.5 K/min. A baseline is made using blank samples containing only water. The results are used to evaluate the ability of AAILs as both THIs and KHIs. The data analysis is interpreted in the following section.

3. Theory and calculation

3.1. Thermodynamic and kinetic methane hydrate inhibition ability analysis

The heat flow spectrum from μ-DSC is utilized to evaluate inhibition ability. Fig. 1 shows an example of the HP μ-DSC spectrum. The exothermic peaks which are the positive peaks represent the ice and hydrate formations. The onset time of the hydrate formation peak is taken as the induction time. The induction time is the time where the first hydrate is formed, and it represents the kinetic methane hydrate inhibition ability of AAILs. Recently, relative inhibition power (RIP) is also used to represent the KHI ability. Thus, the relative inhibition power (RIP) of AAILs is calculated as shown in the following equation:

$$RIP = \frac{induction\ \ time_{AAIL} - induction\ \ time_{water}}{induction\ \ time_{water}}$$

On the other hand, the endothermic peaks which are the negative peaks represent the ice and hydrate dissociation. The offset temperature of the hydrate dissociation peak is taken as the hydrate shifting temperature. The hydrate shifting temperature is the temperature where the final hydrate is dissociated. The offset temperatures are used to plot the HLVE curve. The bigger the shift of the HLVE curve of water containing AAILs from that of water, the higher the THI of the AAILs.

3.2. Study of AAILs molecular properties using COSMO-RS software

Conductor-like Screening Model for Real Solvents (COSMO-RS) is a technique utilizing the unimolecular quantum chemical calculations for predicting the thermophysical properties of liquids mixtures [21]. The geometry optimizations of all AAILs are executed using density functional theory (DFT) approach employing the Becke 3-parameter Lee-Yang-Parr (B3LYP) functional [22] through the resolution of identity (RI) approximation and a triple-ξ valence polarized basis set (TZVP) using TmoleX3.1 (Turbomole Version 6.2) quantum mechanics package [23]. The analysis is done using the COSMOthermX program Version 2.1. The inhibition mechanism of all AAILs towards gas hydrate is evaluated through their screening charge density (σ) profiles or σ-profile [24] through the following equation:

$$p(\sigma) = \frac{\sum_i x_i p^{X_i(\sigma)}}{\sum_i x_i} \quad (2)$$

where $p(\sigma)$ is σ-profile or the distribution of the segments with respect to σ, X_i is compound, x_i is the mole fraction of the compound and $p^{Xi(\sigma)}$ is the relative amount of surface polarity σ for a molecule X_i.

4. Results & discussion

4.1. Validation of experimental procedure and standard correlation model

The HLVE curve of gas hydrate in water is compared with the literature to validate the reliability of the experimental procedure. The result is shown in Fig. 2 where the result of this study is congruent with the literature [25-30]. Besides that, a standard correlation model for the dissociation conditions of methane hydrate in pure water is developed based on our result and literature for a pressure range of 2.9–72.3 MPa. The correlation is expressed as the following equation:

$$T_{Diss} = 8.651 lnP + 265.824 \quad (3)$$

where T_{Diss} is hydrate shifting temperature and P is pressure. The experimental and calculated hydrate shifting temperature in the water of this study is also tabulated in Table 2. The average absolute error is found to be very low at 0.34%.

4.2. Evaluation of the thermodynamic and kinetic hydrate inhibition ability of AAILs

The HLVE curve generated from the hydrate shifting temperature in water and 10 wt% AAILs is shown in Fig. 3. Based on the fig-

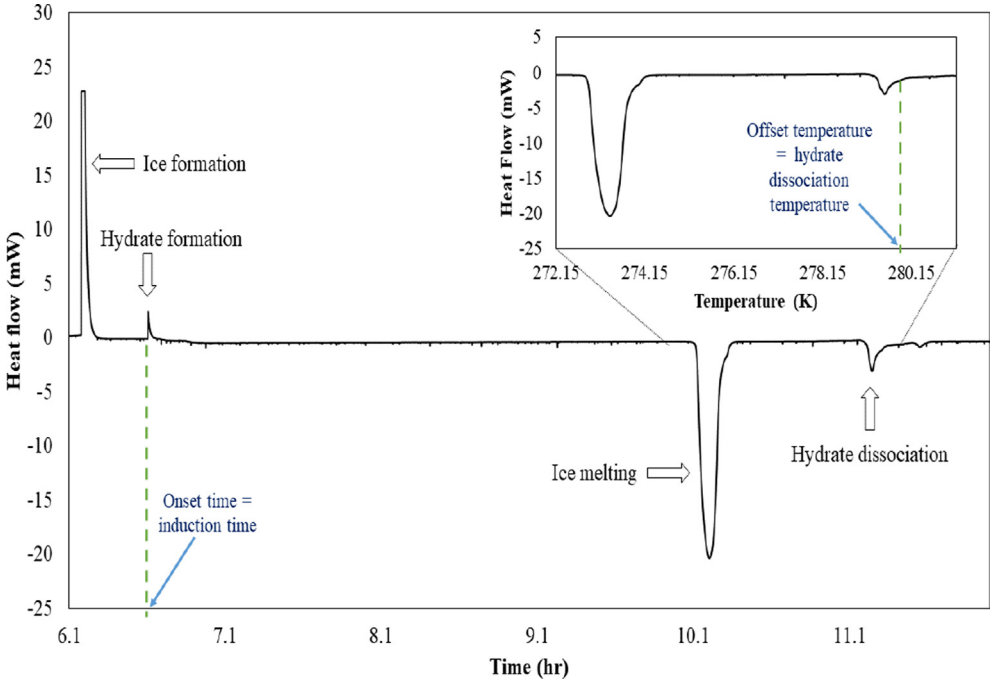

Fig. 1. Example of DSC thermogram of hydrate formation and dissociation.

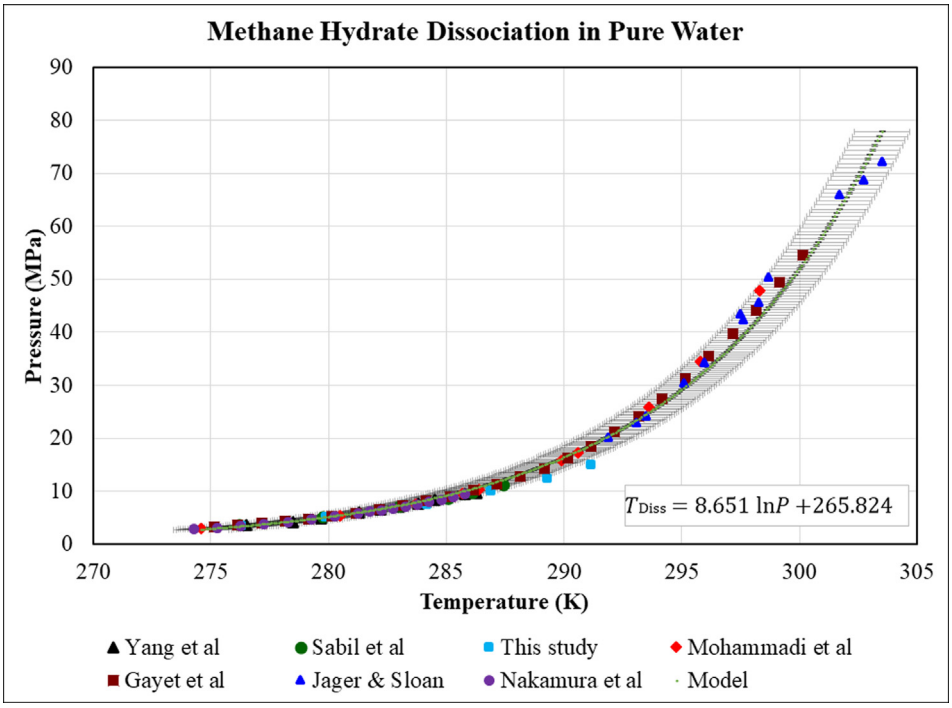

Fig. 2. Hydrate-aqueous Liquid-Vapor Equilibrium (HLVE) curve of methane hydrate in water.

Table 2
Experimental and calculated hydrate shifting temperature in water in this study.

Pressure (MPa)	Shifting Temperature (K)		Absolute error (%)
	Experimental	Calculated	
3.6	276.300	276.905	0.219
5.1	279.855	279.919	0.023
7.6	284.138	283.370	0.271
10.1	286.895	285.830	0.373
12.6	289.250	287.743	0.524
15.1	291.120	289.309	0.626
Average absolute error (%)			0.339

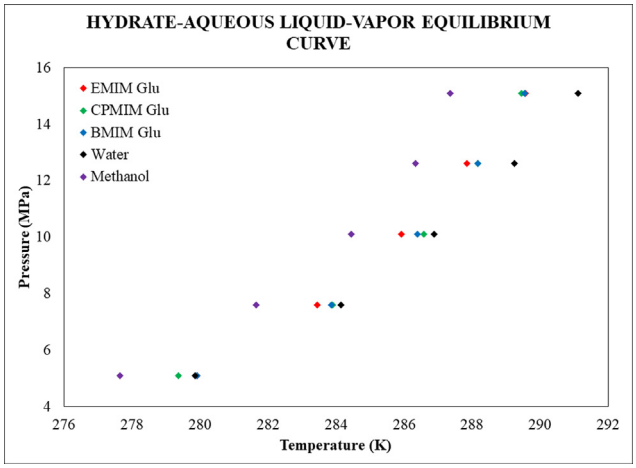

Fig. 3. Hydrate-aqueous Liquid-Vapor Equilibrium (HLVE) curve of methane hydrate in pure water and 10 wt% of various AAILs.

ure, AAILs has shifted the HLVE curve to lower temperature. Hence, they can function as a thermodynamic hydrate inhibitor for methane hydrate. The average shifting temperature of methane hydrate when different ionic liquids are used is also calculated and presented in Table 3. The result shows that EMIMGlu shows the highest dissociation (1.14 K), followed by CPMIMGlu (0.91 K) and BMIMGlu (0.87 K). As a benchmark, the ability of methanol to inhibit methane hydrate is also evaluated where an average shifting temperature of 2.94 K is achieved. Even though the inhibition performance of the studied AAILs is lower than that of methanol, AAILs has negligible vapour pressure. Thus, it can be recovered using a separator. Hence, the use of AAILs may reduce the operating expenses as compared to the methanol system. The induction time is the time when the first methane hydrate was formed, and it represents the KHI ability of the ILs. The relative inhibition power (RIP) is calculated using induction time as tabulated in Table 3. The result shows that CPMIMGlu shows the highest RIP (0.131), followed by EMIMGlu (0.130) and BMIMGlu (0.063).

4.3. Study of hydrate inhibition mechanism by AAILs through COSMO-RS software

To understand the result, the interaction of these AAILs with water is investigated at the molecular level using Turbomole software and Conductor-like Screening Model in Real Solvents (COSMO-RS) software. Their qualitative description such as polarity, non-polarity and hydrogen bonding can be visualized with the help of 3D screening charge distribution [31]. At first, the structures are geometrically optimized using Turbomole software are shown in Fig. 4. For the 3D structure, the green atom is a carbon atom, the blue atom is a nitrogen atom, and the white atom is a hydrogen atom while the red atom is an oxygen atom. For the sigma surface, the red, green and blue surface colours represent negatively, neutral and positively charged moieties. The negatively and positively charged moieties have a high tendency to interact with each other.

The structure of cations, anion and water are imported to COSMO-RS software to further assess the interaction of AAILs with water through charge distribution histograms named σ-profile and σ-potential as shown in Fig. 5 (a) and (b). The σ-profile histogram

Table 3
Average shifting temperature and relative inhibition power (RIP) of hydrate in 10 wt% AAILs.

No.	AAILs	Average shifting temperature (K)	Average induction time (hr)	Relative Inhibition Power
1	EMIM Glu	1.14	5.1	0.130
2	CPMIM Glu	0.91	5.4	0.131
3	BMIM Glu	0.87	4.8	0.063

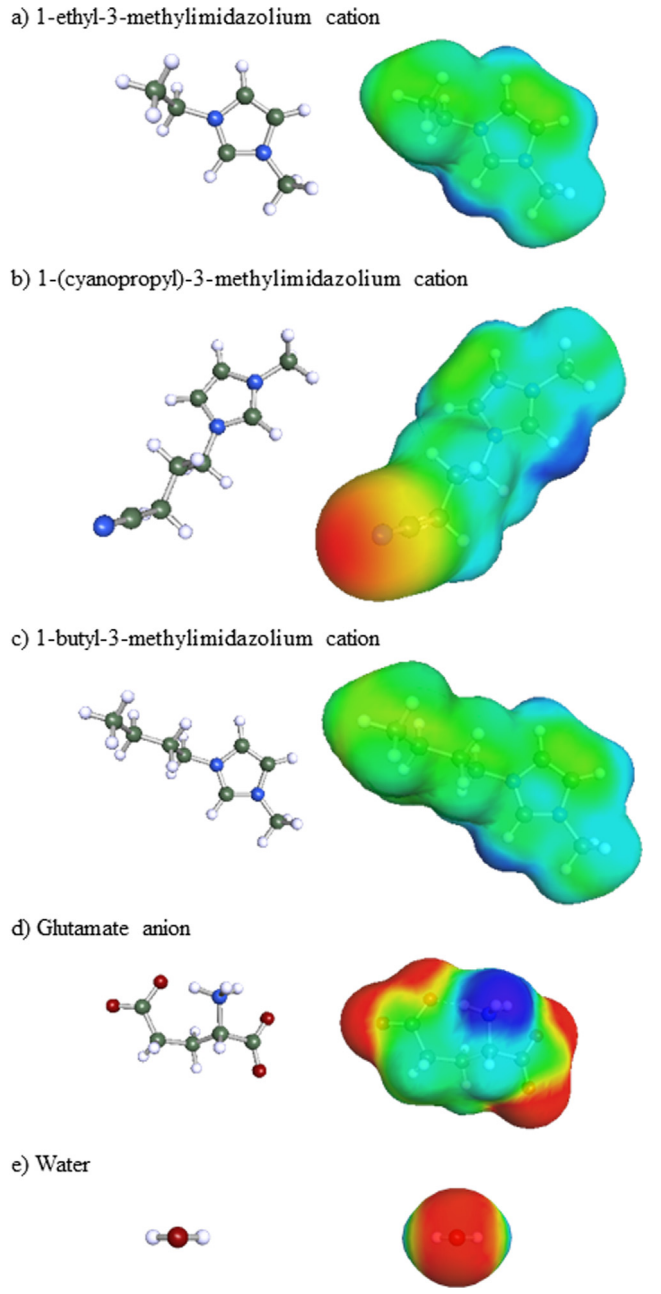

Fig. 4. 3D structure and sigma surface of water, cation, and anion of AAILs used in this study.

defined the properties of the molecules, and it can be evaluated quantitatively by dividing the histogram into three regions. They are the hydrogen-bond donor region, non-polar region and hydrogen-acceptor region [32]. The peaks at hydrogen-bond donor and acceptor regions show a high polarized charge of water which are corresponded to the oxygen atom having electron valence and the hydrogen atom, respectively. All AAILs' histograms also have peaks at the hydrogen-bond acceptor region because the glutamate anion has four oxygen atoms with electron valence. Additionally, CPMIMGlu has an extra peak at the hydrogen-bond acceptor region because of the existence of the cyano group at the end of the alkyl chain. This cyano group has a triple bond and the nitrogen atom has electron valence where they can be hydrogen-bond acceptor group. At the non-polar region, all AAILs have high peaks because of the existence of imidazolium-ring and alkyl chains. However, the height of all peaks, depending on the alkyl chain length. BMIMGlu with a four-carbon alkyl chain has the highest peak due to its long alkyl chain while EMIMGlu with a two-carbon alkyl chain has a shorter peak. The shape of the peak for CPMIMGlu at the non-polar region is slightly different from the others due to the difference in the structure of the cation, where the cyano group exist at the end of its alkyl chain.

Alternatively, the σ-potential histogram represents the interaction of the molecules with other molecules. The left side of the histogram depicts the interaction of the molecule with those having a hydrogen-bond donor atom. The middle side of the histogram depicts the interaction of the molecule with those having non-polar groups. While the right side of the histogram depicts the interaction of the molecule with those having a hydrogen-bond acceptor atom. Increasing negativity of μ (σ) value shows an increasing interaction while an increasing positivity of μ (σ) value shows a decreasing interaction [33]. In Fig. 5 (b), water shows an increasing interaction with molecules having both hydrogen-bond donor and acceptor atoms, due to the existence of an oxygen atom having electron valence and a hydrogen atom, respectively. The water also shows no interaction with molecules having non-polar groups. Alternatively, glutamate based ionic liquids show an increasing interaction with molecules having a hydrogen-bond donor atom, which is because of the existence of glutamate anion having four oxygen atoms with electron valence. Hence, glutamate anion has high interaction with water molecules and may disturb the methane hydrate cage formation. There is also a slight interaction of these AAILs with non-polar groups as a result of the presence of the alkyl chain. A shorter alkyl chain is preferred to increase its polarity and interaction with water which is the main molecule forming the methane hydrate.

For further understanding of the correlation between the molecular properties of ionic liquids with their performance as a thermodynamic and kinetic inhibitor, the area under the curves of the σ-profile of all ionic liquids are plotted as shown in Fig. 6 (a). Interestingly, the pattern observed in the area under the histogram for the non-polar region tends to follow a reverse order when compared to the pattern noticed in the average shifting temperature of ionic liquids which indicate their thermodynamic inhibition behaviour. The opposite trend can be attributed to the decrease in non-polarity of the ionic liquid which subsequently increases their interaction with water, thus facilitating the destabilization of the hydrate cage. To further validate this claim, we evaluated the performance of various ILs having two and four alkyl chains in cation from the literature [3,34] as shown in Fig. 6 (b). The trends are similar to those obtained in this study. Conversely, a somewhat parallel pattern was observed in the area under the

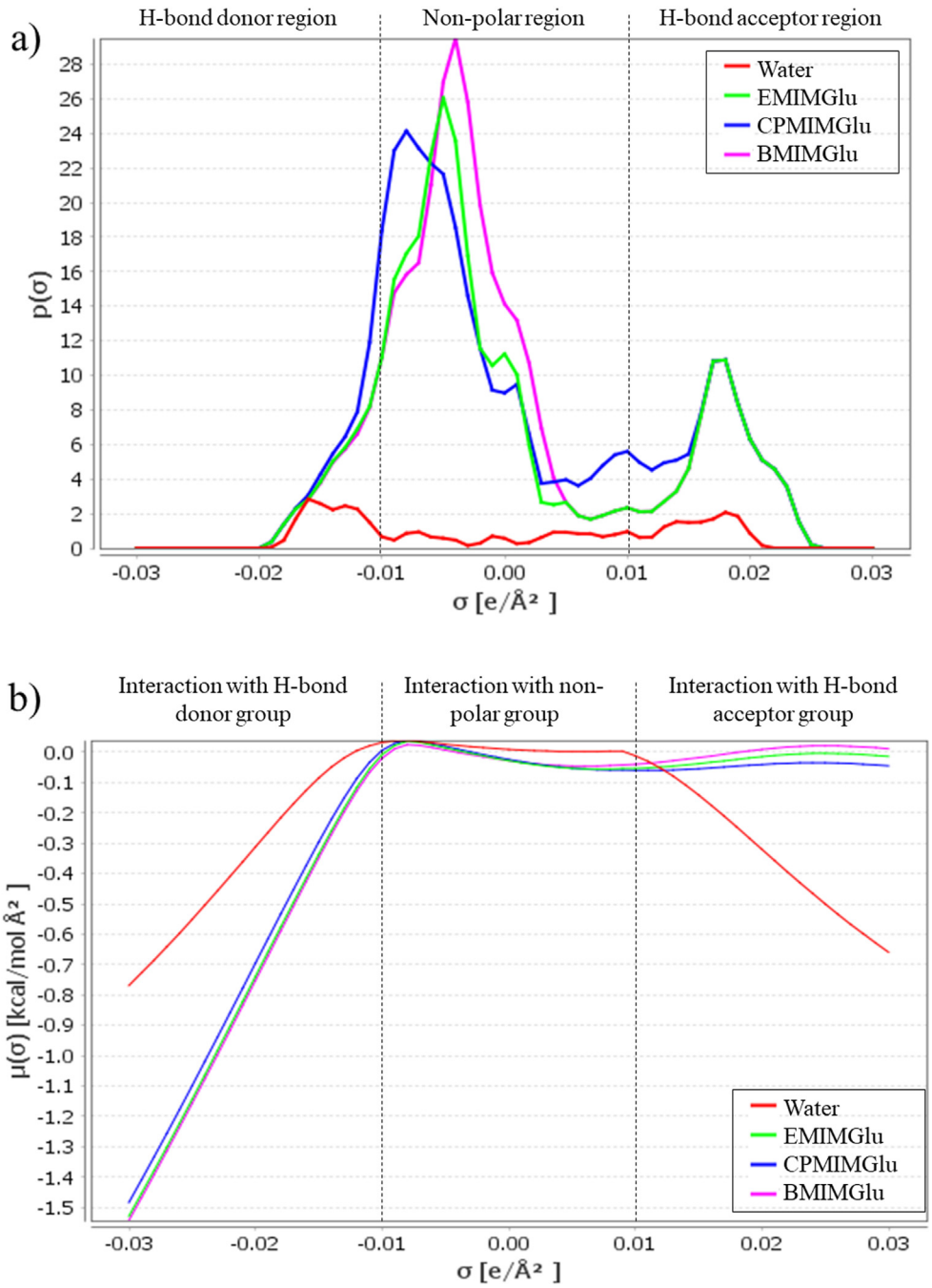

Fig. 5. (a) σ-profile and (b) σ-potential of water, EMIMGlu, CPMIMGlu and BMIMGlu ionic liquids.

histogram for the hydrogen-bond acceptor region and the average induction time of ionic liquids which represents their kinetic inhibition behaviour. An increase in the hydrogen-bond acceptor strength of the ionic liquid increases their interaction with water molecules thereby reducing the hydrate formation. Fig. 6c shows that there exists a good direct correlation between the average induction time and the area under the histogram. Similar observations have been reported in the literature [27,34,35]. Good coefficients of determination were obtained with R^2 of 0.9949 and 0.8598 for the EMIM-based ILs and BMIM-based ILs, respectively. Thus, the average induction time can be predicted from the area under the curve of the hydrogen-bond acceptor region in σ-profile. However, more data is suggested to be evaluated to produce an accurate correlation.

4.4. Dissociation enthalpy for AAILs methane hydrate system

The methane hydrate dissociation enthalpy is determined using the Clausius-Clapeyron as follows:

$$\frac{d(lnP)}{d(T^{-1})} = \frac{-\Delta H_d}{zR} \tag{4}$$

where P is pressure, T is temperature, z is compressibility factor, R is the universal gas constant and ΔH_d is the enthalpy of dissociation. z is determined using the Peng-Robinson equation of state. The dissociation enthalpy is determined from the slope of lnP versus 1/T graph, Enthalpy of methane hydrate dissociation is affected by the crystal hydrogen bonding, hydrate stability and cavity occupation [36]. An assumption was made where the system mainly consists

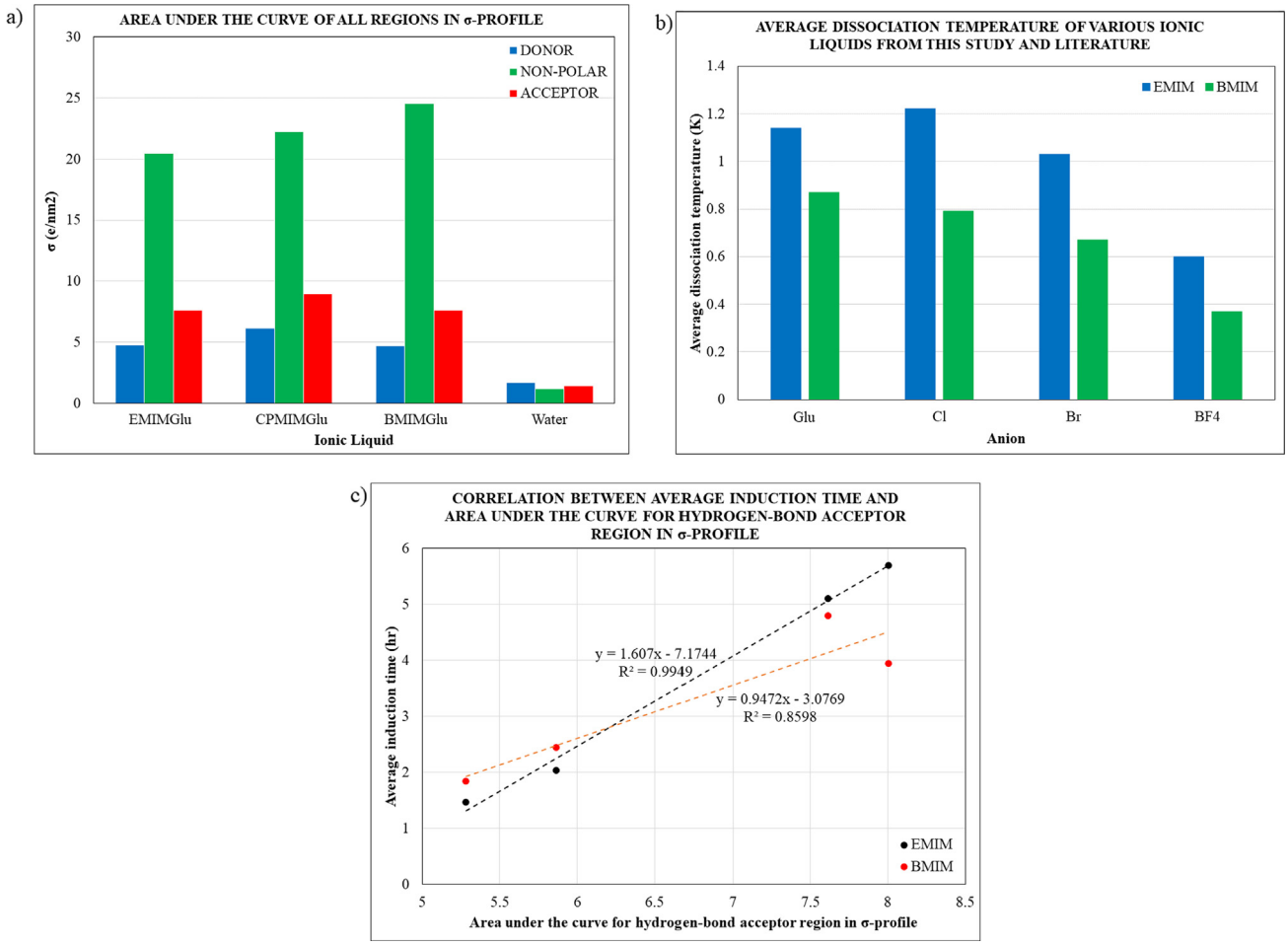

Fig. 6. (a) Area under the curve of all regions in σ-profile, (b) average shifting temperature of various ionic liquids, and (c) correlation between average induction time and area under the curve for hydrogen-bond acceptor region in σ-profile.

of liquid and gas phases at hydrate equilibrium conditions. Thus, the amount of hydrate phase is negligible [37]. The dissociation enthalpy of methane hydrate in water and 10 wt% AAILs are presented in Table 4 and Fig. 7. A nonsignificant change of enthalpy of dissociation defined that the presence of ionic liquid does not give a major effect on the enthalpy of the system [24]. Thus, it does not take part in the methane hydrate structure and cage occupancy. Instead, it only promotes the reduction of water activity to prevent hydrate formation [2]. However, a higher value of enthalpy of dissociation can also be observed which is due to the increase of Gibbs free energy. The increase of Gibbs free energy causes higher pressure or lower temperature requirement to form the methane hydrate [18].

5. Conclusion

A standard correlation of methane hydrate dissociation HLVE curve is successfully developed using the data from this study and literature. The performance of three AAILs is also evaluated in terms of their thermodynamic and kinetic hydrate inhibition ability. All the AAILs show high THIs and KHIs performances. Based on the result of this study and literature, the pattern or trend of THIs performance follows the polarity properties of the ILs while the trend for the KHIs performance follows the hydrogen-bond acceptor properties of the ILs. Therefore, the EMIM-Glu shows the highest thermodynamic hydrate inhibition ability represented by its average shifting temperature, while CPMIM-Glu shows the

Table 4
Dissociation enthalpy of methane hydrate in pure water and 10 wt% of AAILs.

Pressure (MPa)	Enthalpy of dissociation, ΔH (kJ/mol)			
	Pure water	EMIM Glu	CPMIM Glu	BMIM Glu
5.1	56.383	66.365	62.187	65.862
7.6	53.731	63.120	59.279	62.710
10.1	51.862	60.842	57.197	60.476
12.6	50.852	59.550	55.922	59.166
15.1	50.558	59.171	55.483	58.720
Average	*52.677*	*61.809*	*58.014*	*61.387*

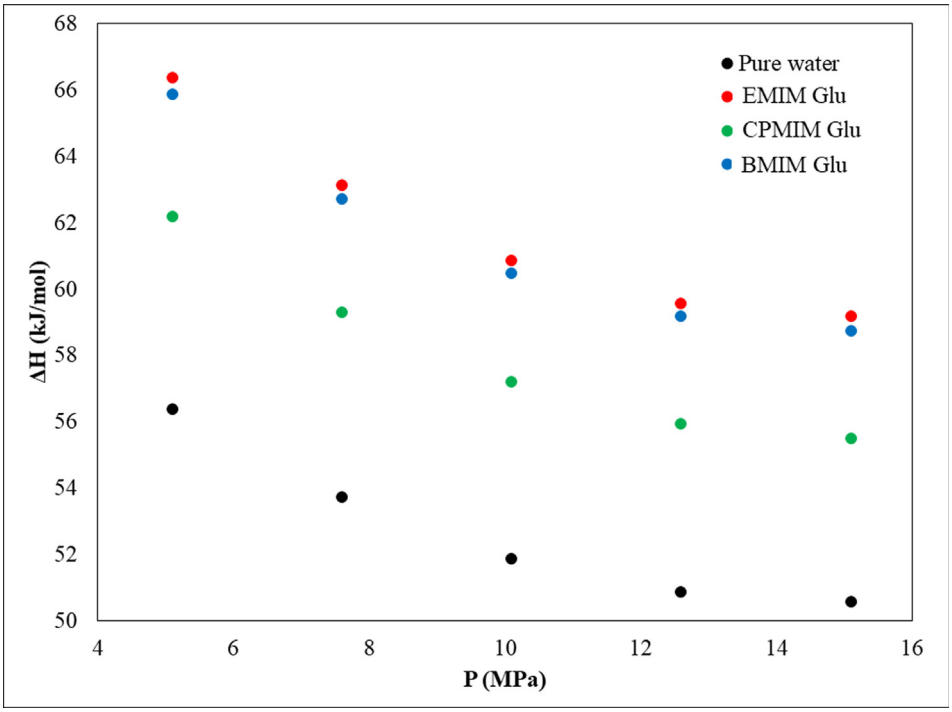

Fig. 7. Hydrate dissociation enthalpies in water and AAILs at different pressures.

highest kinetic hydrate inhibition ability represented by its average induction time and relative inhibition power.

CRediT authorship contribution statement

Asiah Nusaibah Masri: Software, Methodology, Validation, Investigation. **Aliyu Adebayo Sulaimon:** Supervision, Conceptualization, Resources, Funding acquisition.

Declaration of Competing Interest

The authors declare that they have no known competing financial interests or personal relationships that could have appeared to influence the work reported in this paper.

Acknowledgement

The authors acknowledged Yayasan Universiti Teknologi PETRONAS (YUTP 015LC0-102) grant and Universiti Teknologi PETRONAS for their support in conducting this study.

References

[1] E.G. Hammerschmidt, Ind. Eng. Chem. 26 (1934) 851.
[2] E.D. Sloan Jr, C.A. Koh, Clathrate Hydrates of Natural Gases, CRC Press, 2007.
[3] C. Xiao, H. Adidharma, Chem. Eng. Sci. 64 (2009) 1522.
[4] X.-S. Li, Y.-J. Liu, Z.-Y. Zeng, Z.-Y. Chen, G. Li, H.-J. Wu, J. Chem. Eng. Data 56 (2011) 119.
[5] U.S. Energy Information Administration, Washington DC, U.S, 2017.
[6] Q. Nasir, K.K. Lau, B. Lal, K.M. Sabil, J. Chem. Eng. Data 59 (2014) 3920.
[7] M. Tariq, D. Rooney, E. Othman, S. Aparicio, M. Atilhan, M. Khraisheh, Ind. Eng. Chem. Res. 53 (2014) 17855.
[8] A. Eslamimanesh, A.H. Mohammadi, D. Richon, P. Naidoo, D. Ramjugernath, J. Chem. Thermodyn. 46 (2012) 62.
[9] M.S. Kamal, I.A. Hussein, A.S. Sultan, N. von Solms, Renew. Sustain. Energy Rev. 60 (2016) 206.
[10] A.K. Sum, C.A. Koh, E.D. Sloan, Ind. Eng. Chem. Res. 48 (2009) 7457.
[11] M. Cha, K. Shin, Y. Seo, J.-Y. Shin, S.-P. Kang, J. Phys. Chem. A 117 (2013) 13988.
[12] A.N. Masri, A. Mutalib Mi, J.M. Leveque, Ind. Eng. Manage. 05 (2016).
[13] A.N. Masri, M.I. Abdul Mutalib, W.Z.N. Yahya, N.F. Aminuddin, J.M. Leveque, IOP Conf. Ser.: Mater. Sci. Eng. 458 (2018) 012072.
[14] G. Yang, Y. Song, Q. Wang, L. Zhang, L. Deng, Mater. Des. 190 (2020) 108563.
[15] A.N. Masri, M.I. Abdul Mutalib, W.Z.N. Yahya, N.F. Aminuddin, J.M. Leveque, Ultrason. Sonochem. 60 (2020) 104732.
[16] P. Campitelli, M. Aschi, C. Di Nicola, F. Marchetti, R. Pettinari, M. Crucianelli, Appl. Catal. A 599 (2020) 117622.
[17] A.N. Masri, M.I. Abdul Mutalib, N.F. Aminuddin, J.M. Lévêque, Sep. Purif. Technol. 196 (2018) 106.
[18] O. Nashed, D. Dadebayev, M.S. Khan, C.B. Bavoh, B. Lal, A.M. Shariff, J. Mol. Liq. 249 (2018) 886.
[19] P. Gupta, S. Sakthivel, J.S. Sangwai, J. Chem. Thermodyn. 117 (2018) 9.
[20] M. Yu, C.H. Liu, H.H. Zhao, Y.J. Yang, J.H. Sun, Ecotoxicol. Environ. Saf. 190 (2020) 6.
[21] E.I. Alevizou, E.C. Voutsas, Fluid Phase Equilib. 369 (2014) 55.
[22] A. Schäfer, A. Klamt, D. Sattel, J.C.W. Lohrenz, F. Eckert, PCCP 2 (2000) 2187.
[23] K.C. Nicolaou, D. Vourloumis, N. Winssinger, P.S. Baran, Angew. Chem. Int. Ed. 39 (2000) 44.
[24] M.S. Khan, C.B. Bavoh, B. Partoon, B. Lal, M.A. Bustam, A.M. Shariff, J. Mol. Liq. 238 (2017) 533.
[25] S.O. Yang, S.H. Cho, H. Lee, C.S. Lee, Fluid Phase Equilib. 185 (2001) 53.
[26] P. Gayet, C. Dicharry, G. Marion, A. Graciaa, J. Lachaise, A. Nesterov, Chem. Eng. Sci. 60 (2005) 5751.
[27] K.M. Sabil, O. Nashed, B. Lal, L. Ismail, A. Japper-Jaafar, J. Chem. Thermodyn. 84 (2015) 7.
[28] M.D. Jager, E.D. Sloan, Fluid Phase Equilib. 185 (2001) 89.
[29] T. Nakamura, T. Makino, T. Sugahara, K. Ohgaki, Chem. Eng. Sci. 58 (2003) 269.
[30] A.H. Mohammadi, R. Anderson, B. Tohidi, AIChE J. 51 (2005) 2825.
[31] A. Klamt, G. Schüürmann, Journal of the Chemical Society, Perkin Transactions 2 (1993) 799.
[32] Z. Rashid, C. Devi Wilfred, R. Iyyaswami, A. Arunagiri, M. Thanabalan, J. Ind. Eng. Chem. (2019).
[33] K.A. Kurnia, S.P. Pinho, J.A.P. Coutinho, Ind. Eng. Chem. Res. 53 (2014) 12466.
[34] C. Xiao, N. Wibisono, H. Adidharma, Chem. Eng. Sci. 65 (2010) 3080.
[35] M. Zare, A. Haghtalab, A.N. Ahmadi, K. Nazari, Fluid Phase Equilib. 341 (2013) 61.
[36] E.D. Sloan, F. Fleyfel, Fluid Phase Equilib. 76 (1992) 123.
[37] B. Partoon, K.M. Sabil, H. Roslan, B. Lal, L.K. Keong, Fluid Phase Equilib. 412 (2016) 51.